SPECTRAL DECOMPOSITION OF THE TURBULENT SELF-SIMILAR JET AND RECOMPOSITION USING LINEAR DYNAMICS

Phoebe Kuhn
Laboratory for Flow Instabilities and Dynamics
Inst. für Strömungsmechanik und Techn. Akustik
Technische Universität Berlin
10623 Berlin, Germany
phoebe.kuhn@tu-berlin.de

Thomas Ludwig Kaiser
Laboratory for Flow Instabilities and Dynamics
Inst. für Strömungsmechanik und Techn. Akustik
Technische Universität Berlin
10623 Berlin, Germany
t.kaiser@tu-berlin.de

Julio Soria
Laboratory for Turbulence Research
in Aerospace and Combustion (LTRAC)
Monash University
3800 Clayton, VIC, Australia
julio.soria@monash.edu

Kilian Oberleithner
Laboratory for Flow Instabilities and Dynamics
Inst. für Strömungsmechanik und Techn. Akustik
Technische Universität Berlin
10623 Berlin, Germany
oberleithner@tu-berlin.de

ABSTRACT

Coherent structures in the far field of a round turbulent jet at exit Reynolds number $Re = 17\,000$ are investigated experimentally by means of time-resolved 2D-3C PIV in stream-wise and cross-stream sections of the flow. Empirical mode shapes are extracted via spectral proper orthogonal decomposition and the results are compared to two modelling approaches. A local quasi-parallel stability analysis is carried out based on the self-similar velocity profiles and a global optimal response analysis is performed. For both analyses, an eddy viscosity model is employed. The results of both models compare well with the experiments for azimuthal wavenumbers $m = 0$ to $m = \pm 3$ over a wide frequency range. In particular, the optimal response modes show an excellent agreement of up to 98% with the empirical modes, even representing dynamics in the inertial subrange. Within the resolvent framework, non-modal effects are indirectly accounted for and the non-parallelism of the flow does not constitute a restriction to the results as opposed to the quasi-parallel analysis which shows an agreement of up to 95% with the experiments.

INTRODUCTION

The far field of axisymmetric jets has been investigated for many decades due to their basic characteristics and self-similar scaling laws. Although researchers (e.g., Wygnanski *et al.* (1986)) presumed that self-similarity of jets and wakes is connected to the existing coherent structures in the far field, conclusive evidence for this hypothesis has not been provided due to the high requirements on the turbulence data and post processing. In a recent experimental study, the self-similarity of the coherent structures in pipe flows was demonstrated by Hellström *et al.* (2016) which strongly substantiate the connection between self-similarity and coherent structures. For the jet far field, an exact determination of the modal structures and their temporal and spatial behaviour has proven challenging. In the study of Gamard *et al.* (2004), the far field structures were investigated quantitatively and self-similar scaling of the POD eigenspectra was demonstrated and later extended by Wanstrom (2009).

In terms of modelling coherent structures based on linear stability analysis, it is currently unclear whether a linearised modal analysis of the mean flow is applicable to the far field. Considering the near field of natural and forced jets, excellent agreement has been shown in a number of experimental and numerically-based studies (Gudmundsson & Colonius (2011); Oberleithner *et al.* (2014); Cavalieri *et al.* (2013); Beneddine *et al.* (2016)). The following key questions, however, remain open: Which range of turbulent scales are resolved by the eigenmodes of the mean flow and how should the influence of stochastic forcing induced by background turbulence and/or inherent nonlinearities be modelled? The far field of a jet which is self-similar for all turbulent statistical moments, provides an excellent case to address these questions. In a previous study (Kuhn *et al.* (2018)) a modal quasi-parallel linear stability analysis (LSA) was performed and azimuthal mode $m = \pm 1$ was predicted to be the only unstable mode based on a local spatial analysis in self-similar coordinates. However, as shown before by Gamard *et al.* (2004); Wanstrom (2009) and many others, experiments clearly show that the far field comprises a large variation of azimuthal modes over a wide range of frequencies. The objective of this paper is to extend the previous analysis to determine whether a larger proportion of the turbulent spectrum can be modelled correctly via linear dynamics. We address this issue by comparing the experimentally obtained mode shapes to the results of a local quasi-parallel linear stability analysis (LSA) and the optimal response modes of a resolvent analysis.

EXPERIMENTAL SETUP

The experiments were carried out in the water jet test rig shown in figure 2 (Cater & Soria (2002)). The flow is generated by a piston-in-cylinder system which is controlled by a stepper motor-driven lead screw. A high-speed stereoscopic PIV system was used to acquire data at two stream-wise sections (spanning $35 < x/D < 95$) and two cross-stream sections ($x/D = 50$ and $x/D = 80$) of the flow. Water-filled prisms were mounted to the tank walls, to ensure proper optical access and overcome changes in refractive indices. The presented results are derived from cross-stream and stream-wise velocity data of the flow at a Reynolds number of $Re = 17\,000$ based on the nozzle exit bulk velocity of $u_0 = 8$ m/s and the nozzle exit diameter $D = 2.1$ mm.

EMPIRICAL MODE EXTRACTION AND MODELLING APPROACHES

The accurate extraction of coherent structures from measured or simulated flow data of the far field is a challenging task due to their low energy content and the wide spectrum of turbulent scales. To account for this, we apply the frequency-domain spectral proper orthogonal decomposition (SPOD) proposed by Lumley (1967). The SPOD is realised by dividing the time-series into (overlapping) segments, transforming the velocity signal of each segment into frequency domain and subsequently performing a POD for each frequency. Due to the clear frequency separation, this method allows for a consistent comparison with results from analytical models. A Fourier mode decomposition is also discrete in frequency but results in noisy modes for strongly turbulent flows. A comparison of modes extracted via SPOD, Fourier mode decomposition, and time-domain SPOD was presented in a previous investigation (Kuhn *et al.* (2018)) on the same set of velocity data presented here. In order to separate between different azimuthal wavenumbers m, a Fourier transform in the azimuthal direction ($\hat{\mathbf{u}}'(r,t,m) = \int_0^{2\pi} \mathbf{u}'(r,\theta,t)e^{im\theta}d\theta$) is applied to the velocity fields from cross-stream measurements before performing the SPOD.

Within the present study, two approaches are used to model the far field flow structures. A local spatial linear stability analysis (LSA) is carried out in self-similar coordinates based on the measured self-similar velocity profiles. This technique corresponds to an eigenvalue analysis of the averaged equations of motion and continuity using a normal modal ansatz to describe the coherent perturbations. The coherent velocity is described by

$$\tilde{\mathbf{u}}(\mathbf{x},t) = \hat{\mathbf{u}}(r)e^{i(\alpha x + m\theta - \omega t)} + c.c. \tag{1}$$

where α is the complex stream-wise wavenumber, ω the real frequency, m the real azimuthal wavenumber, $\hat{\mathbf{u}}$ the radial amplitude function, and $c.c.$ the corresponding complex conjugate. The perturbation ansatz for the pressure fluctuations is analogous to eq. 1. A more detailed explanation about the numerical approach can be found in Oberleithner *et al.* (2011) and details with regard to the present case are described in Kuhn *et al.* (2018). From the resulting eigenvalue spectrum, the spatially growing ($-\alpha_i > 0$) and decaying ($-\alpha_i < 0$) modes are identified and the mode shape $\hat{\mathbf{u}}$ is determined from the corresponding eigenfunction. The second modelling approach is a global resolvent analysis which is also based on the linearised governing equations of the flow (for details see e.g. Garnaud *et al.* (2013)) but solves an optimisation problem instead of directly examining the stability of the flow. The optimisation parameter is the gain which is defined as $\mu^2 = \frac{||\Psi||_r^2}{||\Phi||_f^2}$ where Φ is an at first arbitrary forcing of the system leading to the response Ψ. The ansatz for perturbation and response modes is harmonic in time and azimuthal direction but not in stream-wise direction:

$$\tilde{\mathbf{q}}(\mathbf{x},t) = \hat{\mathbf{q}}(\mathbf{x})e^{i(m\theta - \omega t)} \tag{2}$$

By optimising the gain μ^2, the resolvent analysis determines the pair of optimal forcing and optimal response, for which the maximum increase of μ^2 is obtained which depends on the chosen norm. In this study, the L^2 norm is applied to the forcing and the response.

Within the present study, the resolvent analysis is performed by the FELICS code using a finite element formulation on an unstructured 2D grid. The mean flow was generated from the measured self-similar velocity profiles in physical coordinates in a domain of $30 < x/D < 900$. The scaling parameters for the mean flow generation are centreline velocity $u_{cl} = Au_0(x/D - x_0/D)^{-1}$ and velocity half-width radius $r_{1/2} = Db(x/D - x_0/D)$. From the experiments the spreading rate was determined to be $b = 0.091$, the decay rate $A = 6.1$, the virtual origin $x_0 = 1.5$, and nozzle bulk velocity is $u_0 = 8$ m/s. Homogeneous Dirichlet boundary conditions were set at the inlet and at $r \to \infty$. The boundary conditions on the jet axis depend on the azimuthal wavenumber.

In order to test the self-similarity of the resulting optimal response modes, several frequencies were evaluated, however, the self-similar state could not be fully confirmed for both forcing and response modes. Possible reasons for this are the upstream boundary condition and the chosen norm that defines the gain μ^2. Instead of using homogeneous Dirichlet boundary conditions, homogeneous Neumann boundary conditions were tested. The results mainly differed in the optimal forcing modes and showed the same inconsistency towards self-similar scaling of the overall spatial amplitude. Nevertheless, self-similarity is very closely achieved in terms of relative magnitudes between the velocity components and also in terms of their phase angles. For the presented results we, therefore, neglect the differences in overall spatial growth.

In both modelling approaches a simple eddy viscosity model was employed. From dimensional considerations, the eddy viscosity can be related to a characteristic length and velocity scale as $\nu_t \sim u^* l^*$. Considering self-similar round jets, the eddy viscosity is determined as $\nu_t = Cu_{cl}r_{1/2}$ which is a constant since $u_{cl} \sim (x - x_0)^{-1}$ and $r_{1/2} \sim (x - x_0)$. Therefore, the eddy viscosity was modelled to be constant and obtained by a fit of the Boussinesq equation $\overline{u'v'} = \nu_t d\bar{u}/dr$ to the experimentally obtained Reynolds shear stress profile.

EXPERIMENTAL AND MODELLING RESULTS

In a previous study (Kuhn *et al.* (2018)) the self-similar flow state of the experiments in the jet far field was analysed and confirmed. Furthermore, a local spatial stability analysis was performed and mode $m = \pm 1$ was found to be the only unstable mode. The present study is focused on the helical $m = 1$ and additionally on the linearly stable modes. Mode shapes from experiment, local stability analysis, and resolvent analysis are compared for azimuthal wavenumbers $m = 0$ to $m = \pm 3$. Higher azimuthal wavenumbers (up to $m = \pm 5$) were also investigated but are not shown here due to space limitations.

A qualitative comparison of mode shapes from experiment, local analysis and resolvent analysis is shown in figure 3 for azimuthal wavenumbers $m = 0$ to $m = 3$ in a cross-sectional plane of the jet. For each azimuthal wavenumber m, the mode shapes of the axial ($\tilde{u}$), radial ($\tilde{v}$) and tangential ($\tilde{w}$) velocity components are displayed and the relative magnitudes/eigenfunctions of the three components are shown in the fourth column normalised by the maximum of the axial component ($|\tilde{u}|$). The top row of each subfigure pictures the empirical mode shapes which correspond to the first SPOD mode. The middle row shows the eigenfunctions from the local analysis and resolvent modes are displayed on the bottom row. All modes are presented at the same self-similar frequency of $\omega^* = 2\pi f r_{1/2}/u_{cl} = 1$. With respect to the local analysis of mode $m = 1$, the selected frequency of $\omega^* = 1$ is outside the unstable domain ($0.02 \leq \omega^* \geq 0.33$) and, thus, in the decaying regime. In figure 3 a good agreement of the two modelling approaches with the empirical modes can be observed at the selected frequency for all shown azimuthal wavenumbers. This agreement also extends to higher azimuthal wavenumbers ($m = 4$ and $m = 5$) which are not shown here. Based on the relative amplitude distribution in the fourth column, a closer match between the optimal response mode and the experiments is observed as opposed to the local analysis.

In order to obtain a more quantitative comparison between experimental results and modelling approaches, the self-similar wavenumber $k^* = kr_{1/2}$, phase velocity $c^*_{ph} = c_{ph}/u_{cl}$ and wavelength $\lambda^* = \lambda/r_{1/2}$ are compared for mode $m = 1$. The wavenumber is determined for empirical modes and optimal response modes by extracting the phase angle $\phi(x)$ on the jet axis (based on the radial velocity component v). Subsequently, the self-similar wavenumber is calculated by $k^* = \frac{d\phi}{dx} r_{1/2}$ and the phase velocity determined as $c_{ph} = \frac{\omega^*}{k^*}$. For the local analysis, the self-similar wavenumber corresponds to the real part of the complex stream-wise wavenumber α^*_r. Figure 4 shows these three quantities plotted against a self-similar axial coordinate x^* which is defined as $x^* = (x - x_0)\sqrt{\frac{f}{u_0 D}}$. The self-similar frequency ω^* is indicated by the top x-axis in figure 4 and is proportional to x^* ($\omega^* \sim x^{*2}$). By linking these two quantities, the self-similarity of the flow allows for interchanging a spatial coordinate with a frequency, i.e. the spatial stream-wise evolution of a wave-packet at a fixed physical frequency f can be interpreted as frequency-dependent evolution at a fixed axial position and vice versa. Comparing the wavenumber k^* and phase velocity c^*_{ph} in figure 4 from the local and the resolvent analysis shows a slightly better agreement of the resolvent analysis with the experiments in a certain self-similar frequency range ($0.2 < \omega^* < 2$) (or corresponding spatial domain). Below this range, a stronger mismatch is observed which is most obvious in the phase velocity c^*_{ph}. We attribute this mismatch to the upstream boundary condition in the resolvent analysis which influences the modal evolution and restricts the self-similarity of the wave-packet as stated in the method section. At higher self-similar frequencies (or further downstream) the results from local analysis and resolvent analysis are identical.

For further quantitative comparison the alignment or congruence between empirical mode shapes and modelling results is computed as proposed by Cavalieri *et al.* (2013). The alignment metric is defined by $\mathcal{M} = \frac{\langle \hat{\mathbf{u}}_{\omega^*,m}, \mathbf{a}_{i=1,\omega^*,m} \rangle}{\|\hat{\mathbf{u}}_{\omega^*,m}\| \, \|\mathbf{a}_{i=1,\omega^*,m}\|}$. Here, $\mathbf{a}_{i=1,\omega^*,m}$ represents the first SPOD mode for azimuthal wavenumber m, and $\hat{\mathbf{u}}_{\omega^*,m}$ are the eigenfunctions from the local analysis or the optimal response mode from the resolvent analysis. A value of $\mathcal{M} = 1$ indicates a perfect match between modelled and empirical modes and $\mathcal{M} = 0$ corresponds to completely uncorrelated mode shapes. In figure 1 the alignment of azimuthal modes $m = 0$ and $m = 1$ is shown in dependence on the self-similar wavenumber k^*. The optimal response modes (dotted lines) show excellent alignment with $\mathcal{M} > 0.95$ over a wide wavenumber range. Only at low wavenumbers the alignment decreases, especially for mode $m = 1$. Furthermore, at very high wavenumbers, the value of $\mathcal{M}$ drops substantially for mode $m = 0$ which can also be observed for $m = 0$ in the local analysis (solid lines). The latter, however, decreases slowly with increasing wavenumber k^* as opposed to the sudden drop obtained for the resolvent modes. In contrast to mode $m = 0$, the values for $\mathcal{M}$ remain at a high and almost identical level for both types of analyses at large wavenumbers k^*. Generally, the level of agreement between local analysis eigenfunctions and empirical modes is slightly lower than for the optimal response modes, especially at low self-similar wavenumbers.

To obtain an idea about what turbulent scales can be modelled with good agreement by both approaches, a turbulent wavenumber spectrum is shown in figure 1b. The spectral density estimates are obtained from spatial Fourier analysis on the jet axis employing self-similar scaling. The data scaling and evaluation procedure is performed following the method of Wanstrom (2009). By comparing the alignment values from figure 1a to the spectral estimates $\Psi_{u,u}$ and Ψ_{vv} in figure 1b, a high degree of agreement can be observed up into the inertial subrange ($k^* > 4$) by both types of analyses.

As a last step, the self-similar wave-packet extracted from experiments are compared to the optimal response mode in figure 5. In each subfigure, the bottom axis corresponds to a self-similar axial coordinate x^* and the top axis constitutes the link to the self-similar frequency ω^*. The first row shows the wave-packet, the second row displays the magnitude and the bottom row the phase angle. In terms of spatial mode shapes and phase angle a good agreement is obtained. However, the overall amplitude which determines the growth of the wave-packet, does not compare well. The resolvent analysis over-predicts the growth of the structures, which grow and decay too far upstream in comparison with the experiments. A similar discrepancy is observed in the linear stability analysis, where the growth rate determines the point of maximum amplitude (neutral point) at a self-similar frequency of $\omega^*_n \approx 0.33$.

CONCLUSIONS

A local spatial stability analysis and global optimal response analysis was performed based on the measured self-similar velocity profiles in the far field of a round turbulent jet. Although only mode $m = 1$ is found to be linearly unstable in the local analysis, good agreement between the empirical and modelled mode shapes is observed for mode $m = 0$ to $m = \pm 3$ over a wide frequency range. The level of agreement between optimal response modes and the ex-

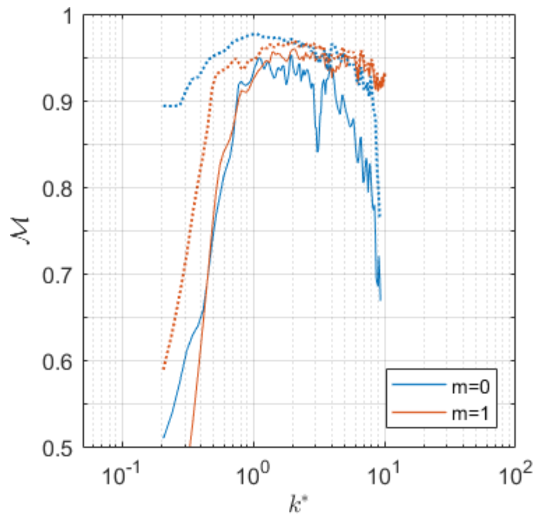

(a) Alignment of optimal response modes (dotted) and local stability analysis (line) with first SPOD modes.

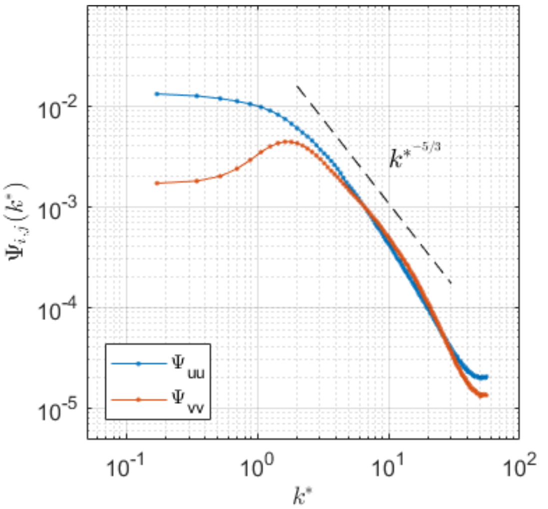

(b) Self-similar wavenumber spectrum determined on jet axis.

Figure 1: Alignment of modes $m = 0$ and $m = 1$ and self-similar turbulent spectrum.

periments is slightly better as this type of analysis can account for effects of non-modal growth and non-parallel base flow. The latter is of particular importance for low frequencies, where the flow is highly non-parallel with respect to the wavelength of the perturbation. For both modelling approaches the same eddy viscosity ansatz was included in the analysis. Without an eddy viscosity, the resulting modes were centred closely around the jet axis and, therewith, differed substantially from the empirical modes (not shown in this study). Considering the optimal response modes, a non self-similar behaviour can be observed which results from the insufficient treatment of the inlet boundary conditions and domain truncation, as well as the definition for the norms which determine the gain function. Within a local resolvent framework, these issues are avoided, however, the non-parallelism of the flow would not be taken into account. Nonetheless, the results of the resolvent analysis reproduce a considerable part of the turbulent fluctuations and reach far into the inertial subrange. Almost over the entire resolved frequency range, the optimal response modes show an excellent agreement of $> 95\%$ with the empirical modes, indicating that data assimilation based on mean velocity fields is possible for a large proportion of the turbulent spectrum.

ACKNOWLEDGEMENTS

The authors would like to acknowledge the research funding by the Australian Government through the Australian Research Council, The Australia-Germany Joint Research Cooperation Scheme an initiative of Universities Australia and the German Academic Exchange Service (DAAD). P. Kuhn was supported by a scholarship within the doctoral students program of the German Academic Exchange Service (DAAD).

REFERENCES

Beneddine, S., Sipp, D., Arnault, A., Dandois, J. & Lesshafft, L. 2016 Conditions for validity of mean flow stability analysis. *Journal of Fluid Mechanics* **798**, 485–504.

Cater, J. E. & Soria, J. 2002 The evolution of round zero-net-mass-flux jets. *Journal of Fluid Mechanics* **472**, 167–200.

Cavalieri, A. V. G., Rodríguez, D., Jordan, P., Colonius, T. & Gervais, Y. 2013 Wavepackets in the velocity field of turbulent jets. *Journal of Fluid Mechanics* **730**, 559–592.

Gamard, S., Jung, D. & George, W. K. 2004 Downstream evolution of the most energetic modes in a turbulent axisymmetric jet at high Reynolds number. Part 2. The far-field region. *Journal of Fluid Mechanics* **514**, 205–230.

Garnaud, X., Lesshafft, L., Schmid, P. J. & Huerre, P. 2013 The preferred mode of incompressible jets : linear frequency response analysis pp. 189–202.

Gudmundsson, K. & Colonius, T. 2011 Instability wave models for the near-field fluctuations of turbulent jets. *Journal of Fluid Mechanics* **689**, 97–128.

Hellström, L. H. O., Marusic, I. & Smits, A. J. 2016 Self-similarity of the large-scale motions in turbulent pipe flow. *Journal of Fluid Mechanics* **792**, R1.

Kuhn, P., Oberleithner, K. & Soria, J. 2018 Identification of coherent structures in the far field of a turbulent jet based on spectral proper orthogonal decomposition of time-resolved PIV snapshots. In *19th International Symposium on Applications of Laser and Imaging Techniques to Fluid Mechanics*. Lisbon, Portugal.

Lumley, J. L. 1967 The Strucure of Inhomogeneous Turbulent Flows. In *Atmospheric Turbulence and Radio Wave Propagation*, pp. 166–178. Publishing House Nauka, Moscow.

Oberleithner, K., Paschereit, C. O. & Wygnanski, I. 2014 On the impact of swirl on the growth of coherent structures. *Journal of Fluid Mechanics* **741**, 156–199.

Oberleithner, K., Sieber, M., Nayeri, C. N. & Paschereit, C. O. 2011 On the control of global modes in swirling jet experiments. *Journal of Physics: Conference Series* **318** (3), 032050.

Wanstrom, M. 2009 Spatial Decompositions of a Fully-developed Turbulent Round Jet Sampled with Particle Image Velocimetry. Phd thesis, Chalmers University of Technology.

Wygnanski, I., Champagne, F. & Marasli, B. 1986 On the large-scale structures in two-dimensional, small-deficit, turbulent wakes. *Journal of Fluid Mechanics* **168**, 31–71.

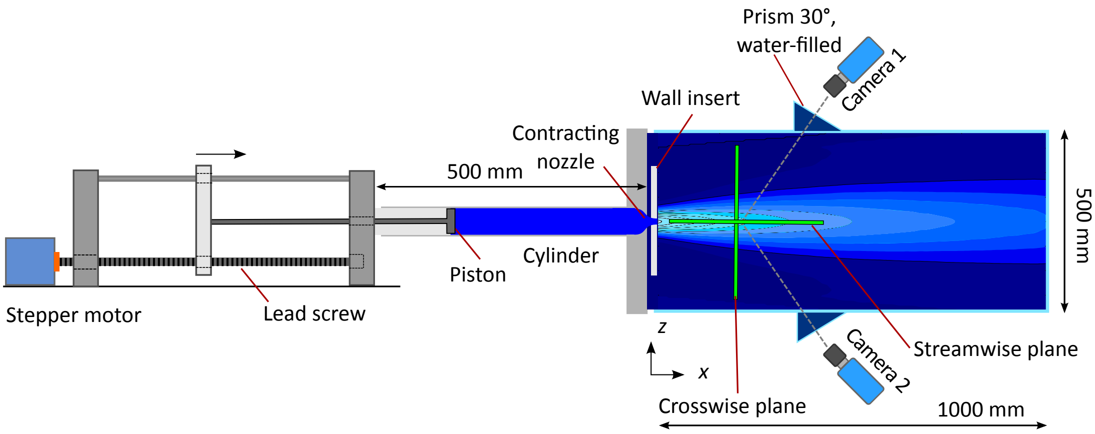

Figure 2: Schematic of the experimental setup

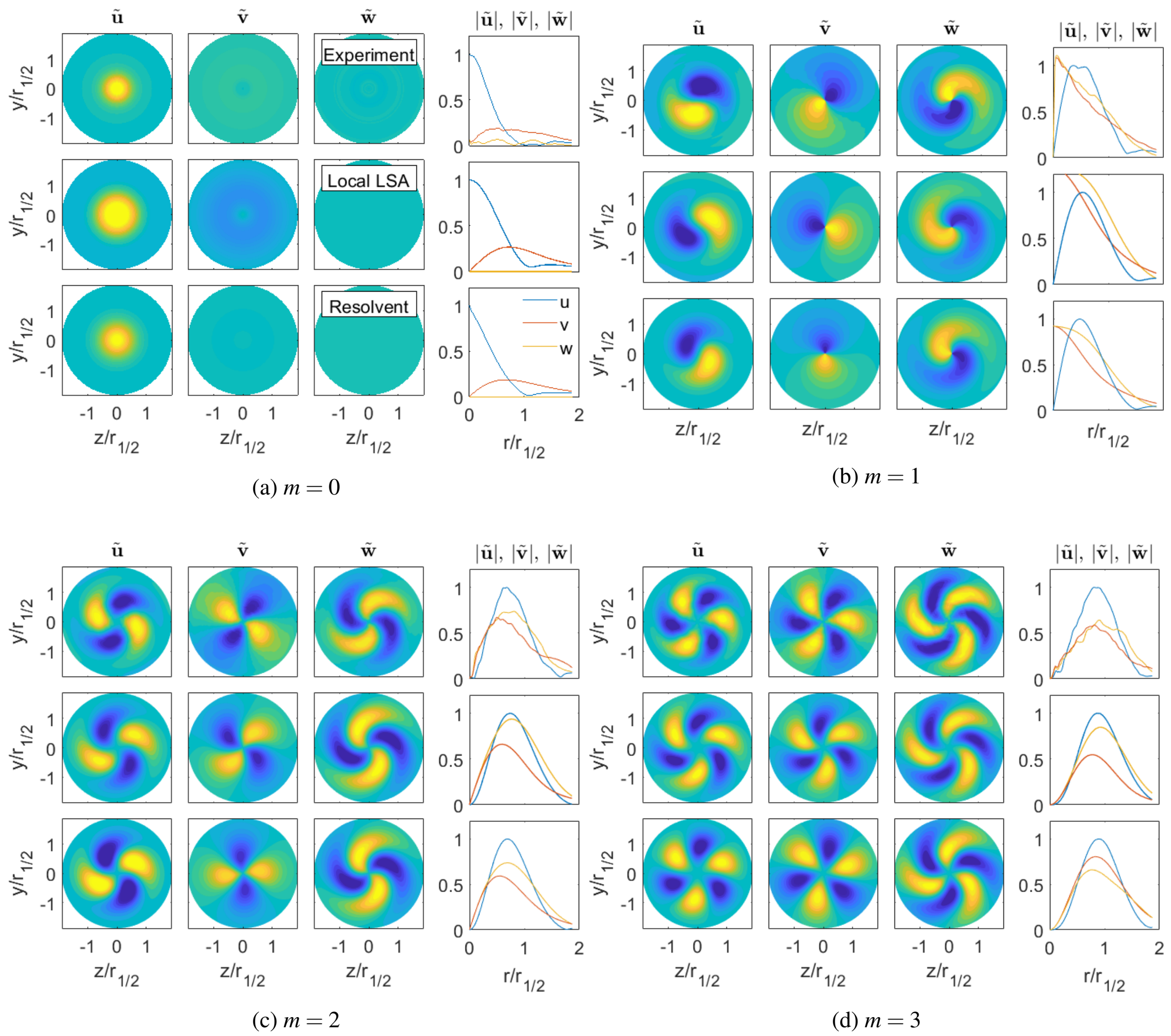

(a) $m = 0$ (b) $m = 1$ (c) $m = 2$ (d) $m = 3$

Figure 3: Cross-stream mode shapes from experiment (top row), local stability analysis (middle row), and resolvent analysis (bottom row) for azimuthal wavenumbers $m = 0$ to $m = 3$. Modes are shown at a self-similar frequency of $\omega^* = 1$.

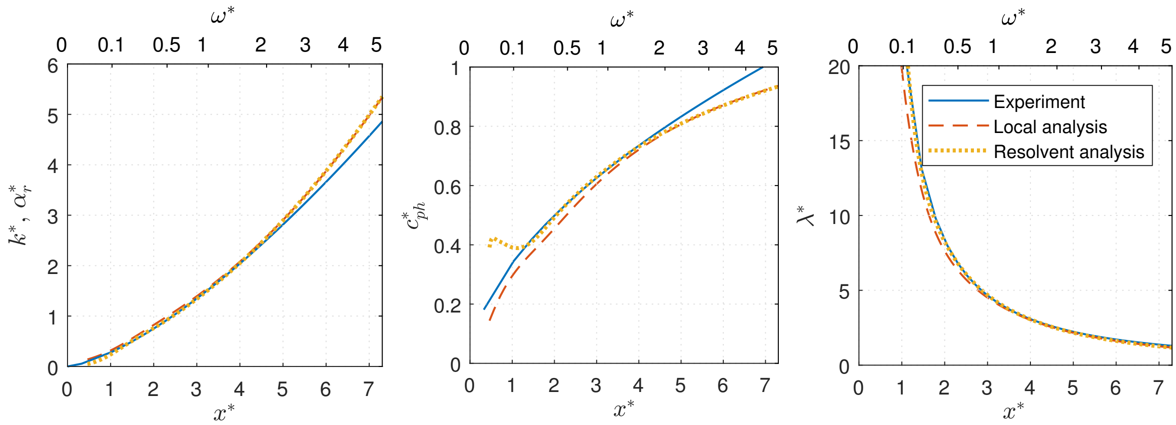

(a) (b) (c)

Figure 4: Comparison of (a) wavenumber k^*, α_r^*, (b) phase velocity c_{ph}^*, and (c) wavelength λ^* from experiment, local LSA, and resolvent analysis for mode $m = 1$.

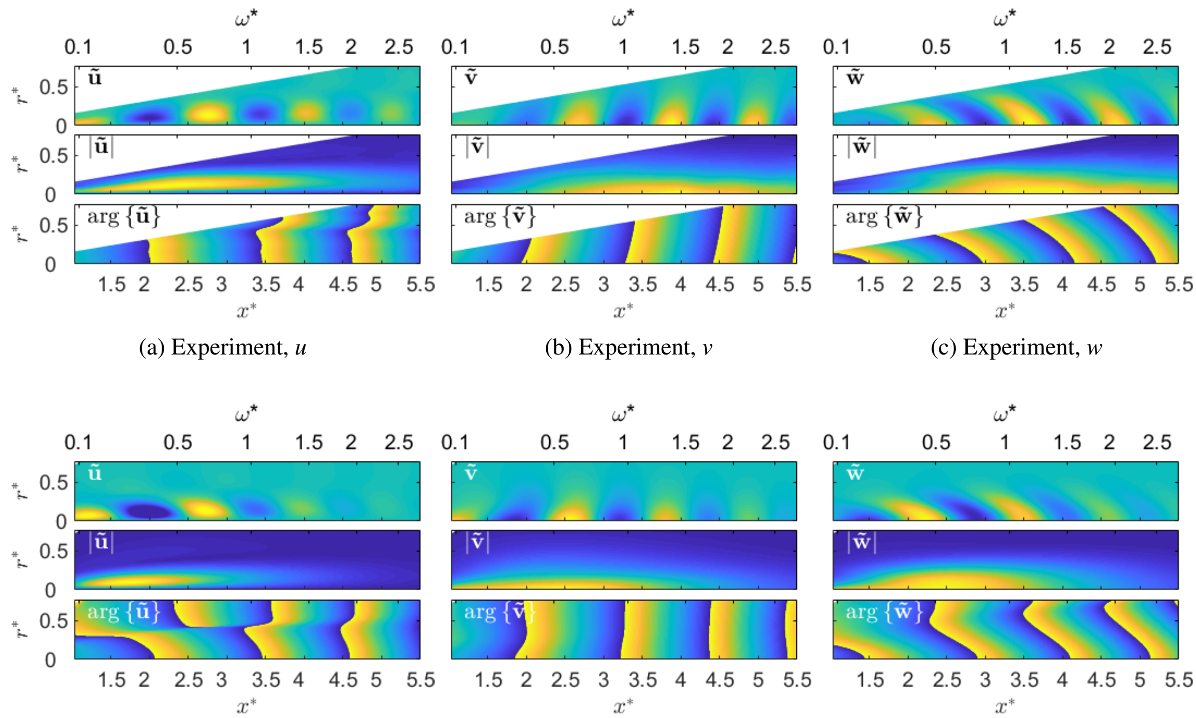

(a) Experiment, u (b) Experiment, v (c) Experiment, w

(d) Optimal response, u (e) Optimal response, v (f) Optimal response w

Figure 5: Streamwise wave-packets from experiment (top) and resolvent analysis (bottom) for axial (u), radial (v), and tangential (w) velocity component.